Chiral-Symmetric Higher-Order Topological Phases of Matter

Wladimir A. Benalcazar[1,2,*] and Alexander Cerjan[3]
[1]Department of Physics, Princeton University, Princeton, New Jersey 08542, USA
[2]Department of Physics, Pennsylvania State University, University Park, Pennsylvania 16802, USA
[3]Center for Integrated Nanotechnologies, Sandia National Laboratories, Albuquerque, New Mexico 87123, USA

(Received 14 September 2021; accepted 17 February 2022; published 23 March 2022)

We introduce novel higher-order topological phases of matter in chiral-symmetric systems (class AIII of the tenfold classification), most of which would be misidentified as trivial by current theories. These phases are protected by "multipole chiral numbers," bulk integer topological invariants that in 2D and 3D are built from sublattice multipole moment operators, as defined herein. The integer value of a multipole chiral number indicates how many degenerate zero-energy states localize at each corner of a system. These higher-order topological phases of matter are generally boundary-obstructed and robust in the presence of chiral-symmetry-preserving disorder.

DOI: 10.1103/PhysRevLett.128.127601

Higher-order topological band theory has expanded the classification of topological phases of matter across insulators [1–13], semimetals [13–18], and superconductors [19–31]. It generalizes the bulk-boundary correspondence of topological phases, so that an nth-order topological phase in d dimensions has protected features, such as gapless states or fractional charges, only at its $(d-n)$-dimensional boundaries. Currently, two complementary mechanisms are known to give rise to higher-order topological phases (HOTPs): (i) corner-induced filling anomalies due to certain Wannier center configurations [2,5,9,32,33] and (ii) the existence of boundary-localized mass domains [2,3,6–8,34,35]. These two mechanisms protect the fractional quantization of corner charge and the existence of single in-gap states at corners, respectively.

In first-order topological systems, phases protecting multiple states at each boundary also exist. This occurs in chiral-symmetric systems (class AIII in the tenfold classification [36–38]) in odd dimensions. In 1D, for example, such phases are identified by a $\mathbb{Z}$ topological invariant known as the winding number [39,40], which classifies the Hamiltonian's homotopy class within the first homotopy group $\pi_1[\mathrm{U}(N)]$ and indicates the number of degenerate zero-energy states at each boundary. In contrast, the Wannier center approach applied to chiral 1D systems only yields a $\mathbb{Z}_2$ classification according to whether the electric dipole moment (given by the position of the Wannier centers) is quantized to 0 or $e/2$. In particular, it labels all 1D chiral-symmetric systems with even winding numbers as trivial.

The observation that 1D systems in class AIII have a broader classification than the one provided by the Wannier center picture suggests that, analogously, a broader classification could exist for HOTPs in class AIII. Consider, for example, stacking N topological quadrupole insulators [1]. If they are coupled in a chiral-symmetric fashion, the overall system will have N zero-energy states protected at each corner. Yet, the topological invariants that protect this phase have not been found. Moreover, the existence of such broader classification would apparently be at odds with the tenfold classification of topological phases, which predicts only trivial phases for chiral-symmetric systems in 2D. This prediction stems from the fact that higher-dimensional generalizations of the 1D winding number—which identify classes within the homotopy group $\pi_d[\mathrm{U}(N)]$ in d-dimensional systems—are trivial for even d [41]. The resolution to this apparent contradiction is that the tenfold classification applies to first-order, bulk-obstructed topological phases, while the phases we consider here are higher order and boundary obstructed. Hence, a different approach is needed to classify chiral-symmetric HOTPs, i.e., one that goes beyond the natural generalization of the 1D winding number to higher dimensions.

In this Letter, we demonstrate the existence of a $\mathbb{Z}$ classification for HOTPs in class AIII and identify the topological invariants in 2D and 3D that protect them. We refer to these invariants as multipole chiral numbers (MCNs) because they generalize the classification provided by the 1D winding number to higher-dimensional systems but, instead of being the traditional generalization of winding numbers to higher dimensions [40], they are built from sublattice multipole moment operators and capture higher-order, boundary-obstructed topology [4,42–46]. These invariants are calculated in the bulk of the system, i.e., with periodic boundary conditions, and, for sufficiently large systems, their integer values indicate the number of degenerate zero-energy states at each corner of a system with open boundaries. Thus, MCNs provide a higher-order bulk-boundary correspondence for topological phases in class AIII. Since MCNs are defined in real space, they can

be used to characterize disordered systems, and here we demonstrate that phases protected by MCNs are robust in the presence of chiral-symmetry-preserving disorder. The existence of phases with MCNs reveals a richer classification of HOTPs, provides a broader understanding of boundary-obstructed topological phases beyond the Wannier center and mass domain perspectives, and has implications for the further classification of HOTPs in interacting systems [47]. The phases we present can be readily proven in several synthetic material platforms [48–51], and recent advances on the generation and control of long-range hoppings could enable their realization in ultracold atoms in optical lattices [52–55].

Let us focus our attention on chiral-symmetric Hamiltonians $\mathcal{H}$, which satisfy $\Pi\mathcal{H}\Pi = -\mathcal{H}$, where Π is the chiral operator. In the basis in which the chiral operator is $\Pi = \tau_z$, the Hamiltonian $\mathcal{H}$ takes the form

$$\mathcal{H} = \begin{pmatrix} 0 & h \\ h^\dagger & 0 \end{pmatrix}, \tag{1}$$

which allows a partition of the lattice into two sublattices, A and B, with opposite chiral charge. The eigenstates of $\mathcal{H}$ can be written as $|\psi_n\rangle = (1/\sqrt{2})(\psi_n^A, \psi_n^B)^T$, where ψ_n^A and ψ_n^B are normalized vectors that exist only in the A and B subspaces, respectively. Under chiral symmetry, every eigenstate $|\psi_n\rangle$ with energy ϵ_n has a chiral partner state $\Pi|\psi_n\rangle = (1/\sqrt{2})(\psi_n^A, -\psi_n^B)^T$ with energy $-\epsilon_n$. Evaluating $\mathcal{H}^2|\psi_n\rangle = \epsilon_n^2|\psi_n\rangle$ leads to the eigenvalue problems $(hh^\dagger)\psi_n^A = \epsilon_n^2\psi_n^A$ and $(h^\dagger h)\psi_n^B = \epsilon_n^2\psi_n^B$, so that ψ_n^A and ψ_n^B can be easily obtained by diagonalizing $hh^\dagger$ or $h^\dagger h$, respectively. This structure is reflected in the singular value decomposition (SVD) of h by writing

$$h = U_A \Sigma U_B^\dagger, \tag{2}$$

where $U_\mathcal{S}$, for $\mathcal{S} = A, B$, is a unitary matrix representing the space spanned by $\{\psi_n^\mathcal{S}\}$, i.e., $U_\mathcal{S} = (\psi_1^\mathcal{S}, \psi_2^\mathcal{S}, \ldots, \psi_{N_\mathcal{S}}^\mathcal{S})$, and Σ is a diagonal matrix containing the singular values. Using this decomposition, it follows that $hh^\dagger = U_A\Sigma^2 U_A^\dagger$ and $h^\dagger h = U_B\Sigma^2 U_B^\dagger$, so that the squared energies $\{\epsilon_n^2\}$ correspond to the squared singular values in Σ^2.

The SVD decomposition (2) allows an explicit flattening of the Hamiltonian by defining the unitary matrix $q = U_A U_B^\dagger$. The winding number of a Bloch Hamiltonian in 1D parametrized by the crystal momentum k is then given by $N_x = (1/2\pi i)\int_{\mathrm{BZ}} \mathrm{Tr}[q(k)^\dagger \partial_k q(k)]$ and is a topological invariant associated with the homotopy classes in $\pi_1[\mathrm{U}(n)] = \mathbb{Z}$.

In the absence of periodicity, k is not a good quantum number and the winding number loses its meaning. However, it is still possible to find real space topological invariants of chiral-symmetric 1D systems (equivalent to the winding number when periodicity is restored), which have allowed for the study of the effects of disorder [56–58]. Specifically, the 1D winding number is equivalent to the real space index $N_x = (1/2\pi i)\mathrm{Tr}\log(\bar{P}_x^A \bar{P}_x^{B\dagger}) \in \mathbb{Z}$, where $\bar{P}_x^\mathcal{S} = U_\mathcal{S}^\dagger P_x^\mathcal{S} U_\mathcal{S}$ is the sublattice dipole operator projected into the spaces $U_\mathcal{S}$, for $\mathcal{S} = A, B$ [57,59]. Here, $P_x^\mathcal{S}$ is defined using the dipole moment operator for periodic systems [60], but restricted to a single sublattice, $P_x^\mathcal{S} = \sum_{R,\alpha\in\mathcal{S}} |R,\alpha\rangle \mathrm{Exp}(-i2\pi R/L)\langle R,\alpha|$, where the 1D crystal has L unit cells, $|R,\alpha\rangle = c_{R,\alpha}^\dagger|0\rangle$, and $c_{R,\alpha}^\dagger$ creates an electron at orbital α of unit cell R.

The MCNs for higher-order topological phases with chiral symmetry are based on extensions of this formulation of real space indices to 2D and 3D. Consider a lattice in 2D (3D) with L_j unit cells along direction $j = x, y$ ($j = x, y$, and z). Each unit cell is labeled by $\mathbf{R} = (x, y)$ [$\mathbf{R} = (x, y, z)$] and has N_T orbitals (or, more generally, N_T internal degrees or freedom). To build the topological indices for chiral-symmetric higher-order topological phases we define the following sublattice multipole moment operators:

$$Q_{xy}^\mathcal{S} = \sum_{\mathbf{R},\alpha\in\mathcal{S}} |\mathbf{R},\alpha\rangle \mathrm{Exp}\left(-i\frac{2\pi xy}{L_x L_y}\right)\langle \mathbf{R},\alpha| \tag{3}$$

$$O_{xyz}^\mathcal{S} = \sum_{\mathbf{R},\alpha\in\mathcal{S}} |\mathbf{R},\alpha\rangle \mathrm{Exp}\left(-i\frac{2\pi xyz}{L_x L_y L_z}\right)\langle \mathbf{R},\alpha|, \tag{4}$$

for 2D and 3D lattices, respectively. These operators resemble those associated with quadrupole and octupole moments [61–63], but are only defined over each sublattice $\mathcal{S} = A, B$, instead of across the entire system.

We claim that the integer invariants for chiral-symmetric second-order topological phases in 2D and third-order topological phases in 3D are, respectively,

$$N_{xy} = \frac{1}{2\pi i}\mathrm{Tr}\log(\bar{Q}_{xy}^A \bar{Q}_{xy}^{B\dagger}) \in \mathbb{Z}, \tag{5}$$

$$N_{xyz} = \frac{1}{2\pi i}\mathrm{Tr}\log(\bar{O}_{xyz}^A \bar{O}_{xyz}^{B\dagger}) \in \mathbb{Z}, \tag{6}$$

where $\bar{Q}_{xy}^\mathcal{S} = U_\mathcal{S}^\dagger Q_{xy}^\mathcal{S} U_\mathcal{S}$ and $\bar{O}_{xyz}^\mathcal{S} = U_\mathcal{S}^\dagger O_{xyz}^\mathcal{S} U_\mathcal{S}$, for $\mathcal{S} = A, B$, are the sublattice multipole moment operators projected into the spaces $U_\mathcal{S}$. To demonstrate that Eqs. (5) and (6) are the invariants for chiral-symmetric higher-order topological phases, one must show that these invariants are strictly quantized, that they predict the number of topologically protected corner states at *each* corner of the lattice, and that phases with different MCNs are separated from one another by phase transitions that close the energy gap.

To prove that the invariants (5) and (6) are strictly quantized, notice that they take the form $N = (1/2\pi i)\mathrm{Tr}\log(U_A^\dagger M_A U_A U_B^\dagger M_B^\dagger U_B)$, where $M_\mathcal{S}$ (for $\mathcal{S} = A, B$) is $Q_{xy}^\mathcal{S}$ in 2D or $O_{xyz}^\mathcal{S}$ in 3D. Since the matrices $M_\mathcal{S}$ and $U_\mathcal{S}$ are unitary, we have $\det(U_A^\dagger M_A U_A U_B^\dagger M_B^\dagger U_B) = \det(M_A M_B^\dagger) = 1$, where the last step follows if the two sublattices have (i) equal number of degrees of freedom in each unit cell and (ii) the same number of unit cells. Under these conditions, tracing the logarithm of $U_A^\dagger M_A U_A U_B^\dagger M_B^\dagger U_B$ will necessarily give a phase that is a multiple of $2\pi i$; i.e., it will be of the form $2\pi i N$, with $N \in \mathbb{Z}$. This integer N is the topological invariant. Exploiting this structure of the invariants, Eqs. (5) and (6) can also be written in the form of a Bott index [64,65], see Supplemental Material [59].

We now illustrate some of the topological phases with nonzero values of N_{xy} and demonstrate that this invariant corresponds to the number of corner-localized states in each corner. Consider the quadrupole topological insulator (QTI) [1] with additional long-range hopping terms. The Bloch Hamiltonian for the QTI has the form of Eq. (1) with the off-diagonal matrix

$$h_{\mathrm{QTI}}(\mathbf{k}) = \begin{pmatrix} -v_x - w_{1,x}e^{-ik_x} & v_y + w_{1,y}e^{ik_y} \\ v_y + w_{1,y}e^{-ik_y} & v_x + w_{1,x}e^{ik_x} \end{pmatrix}, \quad (7)$$

where $v_{x/y}$ and $w_{1,x/y}$ are the nearest-neighbor hoppings within a unit cell and between adjacent unit cells, respectively (generally, we allow for different values of these hoppings in the x and y directions). Adding to this model, we also allow for straight long-range (SLR) hoppings,

$$h_{\mathrm{SLR}}(\mathbf{k}) = \sum_{m>1}^{M} \begin{pmatrix} -w_{m,x}e^{-imk_x} & w_{m,y}e^{imk_y} \\ w_{m,y}e^{-imk_y} & w_{m,x}e^{imk_x} \end{pmatrix}, \quad (8)$$

where M determines the maximum long-range hopping, as well as diagonal long-range (DLR) hoppings,

$$h_{\mathrm{DLR}}(\mathbf{k}) = 2w_D \begin{pmatrix} e^{-ik_x}\cos(k_y) & -e^{ik_y}\cos(k_x) \\ -e^{-ik_y}\cos(k_x) & -e^{ik_x}\cos(k_y) \end{pmatrix}. \quad (9)$$

Here, $w_{m,x/y}$ are the long-range hoppings among the mth nearest-neighbor unit cells in the horizontal and vertical directions, respectively, and w_D are hoppings among nearest-neighbor unit cells along the diagonal directions. All the terms preserve chiral symmetry and the diagonal terms (9) break separability, making it impossible to write the full Hamiltonian as $\mathcal{H}(\mathbf{k}) = \mathcal{H}_x(k_x) + \mathcal{H}_y(k_y)$. In writing this Hamiltonian, we thread a π flux through each plaquette of the system, which is implemented via the specific choice of gauge directly written in Eqs. (7)–(9) and shown in Fig. 1(a).

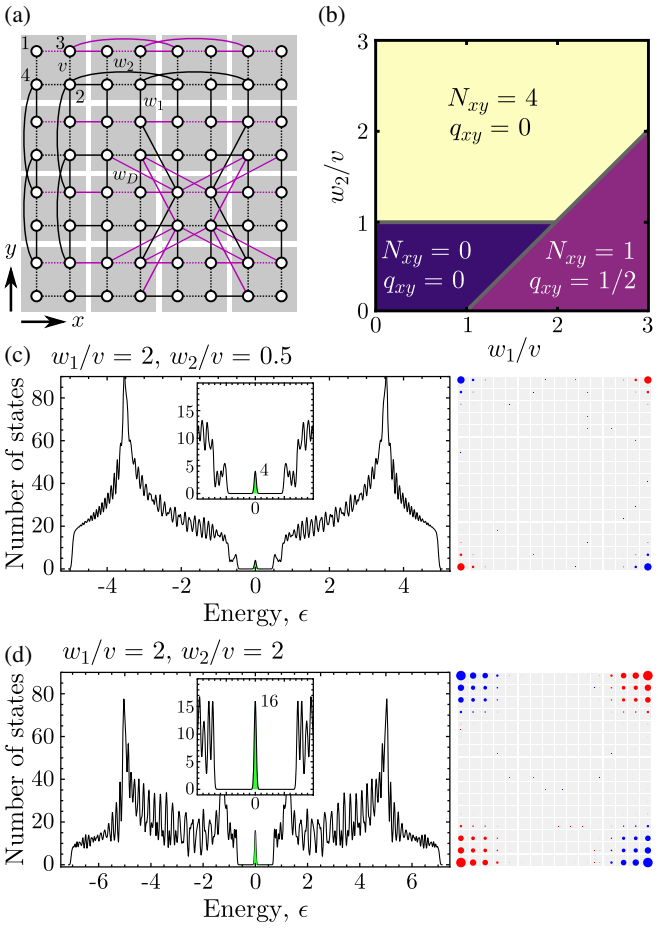

FIG. 1. (a) Schematic depicting the tight-binding model used. Not all non-nearest-neighbor hoppings are shown for clarity. All purple hoppings are multiplied by -1 such that each plaquette has a uniform flux of π. (b) Phase diagram indicating the quadrupole chiral number N_{xy} and the quadrupole moment q_{xy} for a C_{4v}-symmetric system. Here, $w_{m>2} = 0$ and $w_D = 0$. Different phases are separated by gray lines of critical points where the bulk band gap closes. (c),(d) Density of states (left) and local density of states at zero energy (right) for the $N_{xy} = 1$ phase (c) and the $N_{xy} = 4$ phase (d). On the right sides of (c) and (d), red and blue colors indicate support over the A and B sublattices, respectively.

First, consider a chiral and C_4-symmetric, long-range QTI model with $w_{m>2} = 0$ and $w_D = 0$. For $w_m/v < 1$, this system possesses a bulk band gap around zero energy and both the quadrupole moment q_{xy} [1] and the quadrupole winding number N_{xy} [Eq. (5)] identify it as trivial ($q_{xy} = 0$, $N_{xy} = 0$), Fig. 1(b). Starting from this phase and increasing w_1/v, a bulk band-gap-closing phase transition occurs, after which both topological indices now show that this system is in a nontrivial phase ($q_{xy} = 1/2$, $N_{xy} = 1$). With open boundaries, this phase possesses a single zero-energy state localized to each of its corners, Fig. 1(c). This is the previously known QTI phase [1]. However, when the long-range hopping w_2/v is increased, a separate bulk band-gap-closing phase transition occurs that separates

either the $N_{xy} = 0$ phase or the $N_{xy} = 1$ phase from another nontrivial phase with $N_{xy} = 4$, but with $q_{xy} = 0$. Simulations of the open system reveal that each corner of the lattice in this phase possesses four degenerate states with $\epsilon = 0$ and that all such states within a corner exist only on a single sublattice of the system, see Fig. 1(d) and Fig. S2 in the Supplemental Material [59].

Since all of the zero-energy states within a corner occupy the same sublattice, they have the same chiral charge $\Pi|\psi_{\text{corner}}\rangle = \pm|\psi_{\text{corner}}\rangle$ and, thus, cannot pair to hybridize away from zero energy as long as chiral symmetry is preserved.

Not only is the $N_{xy} = 4$ phase not captured by the quadrupole index, but more generally, it lies beyond the framework of induced band representations [66,67]. Consequently, topological indices based on calculating the representations of the bulk bands at high-symmetry points of the Brillouin zone will fail to find this phase, as the representations of the lowest two bands at all of the high-symmetry points are identical in the $N_{xy} = 4$ phase, leading to trivial symmetry indicator invariants, see Supplemental Material [59].

Phase transitions between phases with different MCNs need not close the bulk band gap but, at a minimum, must close some lower-dimensional edge or surface band gap. HOTPs with this property are known as boundary-obstructed topological phases [42]. This property remains true even in the presence of C_4 symmetry, which renders the QTI phase bulk obstructed. For example, consider adding diagonal long-range hoppings to this model, $w_D/v = 0.5$ [Eq. (9)], which preserve chiral and C_4 symmetries but break separability. As can be seen in Fig. 2(a), the $N_{xy} = -1$ and $N_{xy} = 3$ phases each have a phase boundary in which the bulk band gap closes and boundaries with other phases where only the edge band gap closes. Both of these types of boundaries can be explicitly seen in the density of states across these phase transitions, Fig. 2(b). For all of the different phases identified in Fig. 2(a), the number of states localized in each corner of the system is equal to $|N_{xy}|$ and the sublattice over which the corner states are supported is given by $\text{sgn}(N_{xy})$. Thus, for example, the $N_{xy} = -1$ phase in Fig. 2(a) indicates that the system possesses one state localized in each corner with support only on the *opposite* sublattice when compared with those in phases with $N_{xy} > 0$, see Supplemental Material [59]. In 3D, chiral-symmetric higher-order phases are characterized by distinct integer values of Eq. (6), which indicate the number of degenerate states localized at each corner in the 3D structure.

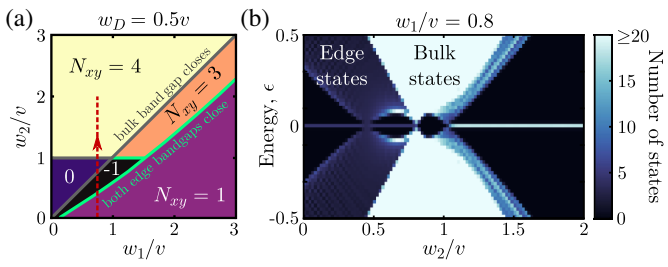

FIG. 2. (a) Phase diagram of the N_{xy} phases for a C_{4v}-symmetric, separability-broken system with $w_D/v = 0.5$ and $w_{m>2} = 0$. Bulk-obstructed phase transitions are shown in gray, while boundary-obstructed phase transitions are shown in lime. (b) Density of states for this system for fixed $w_1/v = 0.8$, indicated as the red line in (a).

Even though the phases shown in Figs. 1 and 2 preserve crystalline symmetries, phases with nonzero MCNs are robust in the presence of short-range correlated disorder that breaks crystalline symmetries. To demonstrate this, we add disorder to the nearest-neighbor hopping coefficients of this model. In particular, we consider a uniform lattice with C_4 symmetry, whose disorder then breaks all spatial symmetries, as well as time-reversal symmetry, by taking values $v_{ij} \to v_{ij} + (W/\sqrt{2})(\xi^{(\text{Re})}_{0,ij} + i\xi^{(\text{Im})}_{0,ij})$ and $w_{1,ij} \to w_{1,ij} + (W/2\sqrt{2})(\xi^{(\text{Re})}_{1,ij} + i\xi^{(\text{Im})}_{1,ij})$, which for sufficiently large disorder strength W causes a phase transition into a trivial phase. Here, $\xi \in [-1, 1]$ are uniformly distributed random numbers and v_{ij} and $w_{1,ij}$ are the hopping strengths between neighboring lattice sites i, j within the same unit cell and between adjacent unit cells, respectively. As can be seen in Fig. 3, an $N_{xy} = 4$ phase remains strictly quantized until a transition drives the system into a trivial phase with $N_{xy} = 0$ when the disorder becomes sufficiently strong. This transition coincides with both bulk and edge band gap closings (up to finite size effects, see Supplemental Material [59]).

Recently, several studies have shown that chiral symmetry alone quantizes quadrupole and octupole moments in insulators [68–70]. Our results show that protection solely due to chiral symmetry also applies to the larger family of topological phases protected by MCNs. This must be the case as systems with different MCNs also possess different

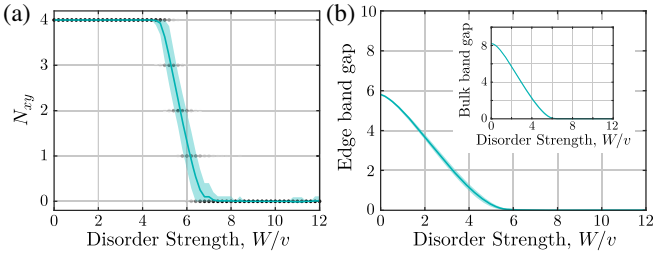

FIG. 3. Numerically calculated N_{xy} (a), edge band gap (b), and bulk band gap (inset), as a function of disorder strength W/v for 100 independent realizations for the disorder on a 40×40 square lattice whose underlying ordered system has $w_1/v = 1$, $w_2/v = 4$, and $w_{m>2} = w_D = 0$. The shading of the points in (a) is proportional to the number of disorder realizations that yield that invariant. The solid line and shaded region show the average of the plotted quantity and the region within 1 standard deviation of the average, respectively.

numbers of topological zero-energy states at each corner; thus, to transition between them, extended zero-energy channels must exist through which some topological states delocalize and hybridize away from zero energy. Such channels are provided by bulk or boundary closings of the energy gap.

Higher-order topological phases have been found in bismuth [71] and Bi_4Br_4 [72]. More recently, the mechanisms for the protection and confinement of modes of higher-order topology have found fertile ground in photonics, acoustics, and topoelectric circuits [48,50,73–81], where they can be used to create robust cavities [82,83] and lasers [84,85]. In fact, since chiral-symmetric HOTPs with large MCNs require increasingly stronger longer-range hoppings, these phases may be hard to attain in solid-state systems, where the electron's hoppings attenuate with separation. However, these phases are readily accessible in microwave photonic resonator arrays [48,49], topoelectric circuits [50], or sonic crystals [51], all of which can implement deformable lattice sites and couplers, which enables separating the geometric configuration of the lattice from the strength of the couplings of resonating states, thus easily achieving long-range couplings [49,51]. Another candidate platform is ultracold atoms in optical lattices, where the realization synthetic gauge fields [52–54] and modulation of hopping terms [52] in 2D has been experimentally shown. Adding long-range hoppings to this platform has been long sought after, and a recent a proposal has been put forward [55] that could give this platform access to the phases we present.

We thank Frank Schindler, Chaoxing Liu, and Shinsei Ryu for interesting discussions. W. A. B. is thankful for the support of the Moore Postdoctoral Fellowship at Princeton University and the Eberly Postdoctoral Fellowship at the Pennsylvania State University. A. C. acknowledges support from the Center for Integrated Nanotechnologies, an Office of Science User Facility operated for the U.S. Department of Energy (DOE) Office of Science, and the Laboratory Directed Research and Development program at Sandia National Laboratories. Sandia National Laboratories is a multimission laboratory managed and operated by National Technology and Engineering Solutions of Sandia, LLC, a wholly owned subsidiary of Honeywell International, Inc., for the U.S. DOEs National Nuclear Security Administration under Award No. DE-NA-0003525. The views expressed in the article do not necessarily represent the views of the U.S. DOE or the U.S. Government.

*wb7707@princeton.edu

[1] W. A. Benalcazar, B. A. Bernevig, and T. L. Hughes, Quantized electric multipole insulators, Science **357**, 61 (2017).
[2] Z. Song, Z. Fang, and C. Fang, $(d-2)$-Dimensional Edge States of Rotation Symmetry Protected Topological States, Phys. Rev. Lett. **119**, 246402 (2017).
[3] J. Langbehn, Y. Peng, L. Trifunovic, F. von Oppen, and P. W. Brouwer, Reflection Symmetric Second-Order Topological Insulators and Superconductors, Phys. Rev. Lett. **119**, 246401 (2017).
[4] W. A. Benalcazar, B. A. Bernevig, and T. L. Hughes, Electric multipole moments, topological multipole moment pumping, and chiral hinge states in crystalline insulators, Phys. Rev. B **96**, 245115 (2017).
[5] G. van Miertand and C. Ortix, Higher-order topological insulators protected by inversion and rotoinversion symmetries, Phys. Rev. B **98**, 081110(R) (2018).
[6] F. Schindler, A. M. Cook, M. G. Vergniory, Z. Wang, S. S. P. Parkin, B. A. Bernevig, and T. Neupert, Higher-order topological insulators, Sci. Adv. **4**, eaat0346 (2018).
[7] E. Khalaf, Higher-order topological insulators and superconductors protected by inversion symmetry, Phys. Rev. B **97**, 205136 (2018).
[8] M. Geier, L. Trifunovic, M. Hoskam, and P. W. Brouwer, Second-order topological insulators and superconductors with an order-two crystalline symmetry, Phys. Rev. B **97**, 205135 (2018).
[9] W. A. Benalcazar, T. Li, and T. L. Hughes, Quantization of fractional corner charge in C_n-symmetric higher-order topological crystalline insulators, Phys. Rev. B **99**, 245151 (2019).
[10] C. Yue, Y. Xu, Z. Song, H. Weng, Y.-M. Lu, C. Fang, and X. Dai, Symmetry-enforced chiral hinge states and surface quantum anomalous hall effect in the magnetic axion insulator $Bi_{2-x}Sm_xSe_3$, Nat. Phys. **15**, 577 (2019).
[11] Y. Xu, Z. Song, Z. Wang, H. Weng, and X. Dai, Higher-Order Topology of the Axion Insulator $EuIn_2As_2$, Phys. Rev. Lett. **122**, 256402 (2019).
[12] L. Elcoro, B. J. Wieder, Z. Song, Y. Xu, B. Bradlyn, and B. A. Bernevig, Magnetic topological quantum chemistry, Nat. Commun. **12**, 5965 (2021).
[13] Y. Xu, L. Elcoro, Z.-D. Song, B. J. Wieder, M. G. Vergniory, N. Regnault, Y. Chen, C. Felser, and B. A. Bernevig, High-throughput calculations of magnetic topological materials, Nature (London) **586**, 702 (2020).
[14] M. Linand and T. L. Hughes, Topological quadrupolar semimetals, Phys. Rev. B **98**, 241103(R) (2018).
[15] J. Ahn, D. Kim, Y. Kim, and B.-J. Yang, Band Topology and Linking Structure of Nodal Line Semimetals with Z_2 Monopole Charges, Phys. Rev. Lett. **121**, 106403 (2018).
[16] Z. Wang, B. J. Wieder, J. Li, B. Yan, and B. A. Bernevig, Higher-Order Topology, Monopole Nodal Lines, and the Origin of Large Fermi Arcs in Transition Metal Sichalcogenides XTe_2 (X = Mo, W), Phys. Rev. Lett. **123**, 186401 (2019).
[17] B. J. Wieder, Z. Wang, J. Cano, X. Dai, L. M. Schoop, B. Bradlyn, and B. A. Bernevig, Strong and fragile topological dirac semimetals with higher-order Fermi arcs, Nat. Commun. **11**, 627 (2020).
[18] Sayed Ali Akbar Ghorashi, T. Li, and T. L. Hughes, Higher-Order Weyl Semimetals, Phys. Rev. Lett. **125**, 266804 (2020).
[19] W. A. Benalcazar, J. C. Y. Teo, and T. L. Hughes, Classification of two-dimensional topological crystalline superconductors and Majorana bound states at disclinations, Phys. Rev. B **89**, 224503 (2014).

[20] Y. Wang, M. Lin, and T. L. Hughes, Weak-pairing higher order topological superconductors, Phys. Rev. B **98**, 165144 (2018).

[21] T. Liu, J. J. He, and F. Nori, Majorana corner states in a two-dimensional magnetic topological insulator on a high-temperature superconductor, Phys. Rev. B **98**, 245413 (2018).

[22] V. Dwivedi, C. Hickey, T. Eschmann, and S. Trebst, Majorana corner modes in a second-order Kitaev spin liquid, Phys. Rev. B **98**, 054432 (2018).

[23] X. Zhu, Tunable Majorana corner states in a two-dimensional second-order topological superconductor induced by magnetic fields, Phys. Rev. B **97**, 205134 (2018).

[24] C.-H. Hsu, P. Stano, J. Klinovaja, and D. Loss, Majorana Kramers Pairs in Higher-Order Topological Insulators, Phys. Rev. Lett. **121**, 196801 (2018).

[25] S. A. A. Ghorashi, T. L. Hughes, and E. Rossi, Vortex and Surface Phase Transitions in Superconducting Higher-Order Topological Insulators, Phys. Rev. Lett. **125**, 037001 (2020).

[26] S. Franca, D. V. Efremov, and I. C. Fulga, Phase-tunable second-order topological superconductor, Phys. Rev. B **100**, 075415 (2019).

[27] Z. Yan, Higher-Order Topological Odd-Parity Superconductors, Phys. Rev. Lett. **123**, 177001 (2019).

[28] Y. Volpez, D. Loss, and J. Klinovaja, Second-Order Topological Superconductivity in π-Junction Rashba Layers, Phys. Rev. Lett. **122**, 126402 (2019).

[29] R.-X. Zhang, J. D. Sau, and S. D. Sarma, Kitaev building-block construction for higher-order topological superconductors, arXiv:2003.02559.

[30] D. Vu, R.-X. Zhang, and S. D. Sarma, Time-reversal-invariant c_2-symmetric higher-order topological superconductors, Phys. Rev. Research **2**, 043223 (2020).

[31] F. Schindler, B. Bradlyn, M. H. Fischer, and T. Neupert, Pairing Obstructions in Topological Superconductors, Phys. Rev. Lett. **124**, 247001 (2020).

[32] Y. Fangand and J. Cano, Filling anomaly for general two- and three-dimensional C_4 symmetric lattices, Phys. Rev. B **103**, 165109 (2021).

[33] R. Takahashi, T. Zhang, and S. Murakami, General corner charge formula in two-dimensional C_n-symmetric higher-order topological insulators, Phys. Rev. B **103**, 205123 (2021).

[34] E. Khalaf, H. C. Po, A. Vishwanath, and H. Watanabe, Symmetry Indicators and Anomalous Surface States of Topological Crystalline Insulators, Phys. Rev. X **8**, 031070 (2018).

[35] L. Trifunovicand and P. W. Brouwer, Higher-Order Bulk-Boundary Correspondence for Topological Crystalline Phases, Phys. Rev. X **9**, 011012 (2019).

[36] A. P. Schnyder, S. Ryu, A. Furusaki, and A. W. W. Ludwig, Classification of topological insulators and superconductors in three spatial dimensions, Phys. Rev. B **78**, 195125 (2008).

[37] A. Kitaev, Periodic table for topological insulators and superconductors, AIP Conf. Proc. **1134**, 22 (2009).

[38] S. Ryu, A. P. Schnyder, A. Furusaki, and A. W. W. Ludwig, Topological insulators and superconductors: Tenfold way and dimensional hierarchy, New J. Phys. **12**, 065010 (2010).

[39] S. Ryuand and Y. Hatsugai, Topological Origin of Zero-Energy Edge States in Particle-Hole Symmetric Systems, Phys. Rev. Lett. **89**, 077002 (2002).

[40] J. C. Y. Teoand and C. L. Kane, Topological defects and gapless modes in insulators and superconductors, Phys. Rev. B **82**, 115120 (2010).

[41] M. Nakahara, *Geometry, Topology and Physics*, 2nd ed. (CRC Press, Boca Raton, FL, 2003).

[42] E. Khalaf, W. A. Benalcazar, T. L. Hughes, and R. Queiroz, Boundary-obstructed topological phases, Phys. Rev. Research **3**, 013239 (2021).

[43] M. Ezawa, Edge-corner correspondence: Boundary-obstructed topological phases with chiral symmetry, Phys. Rev. B **102**, 121405(R) (2020).

[44] A. Tiwari, A. Jahin, and Y. Wang, Chiral Dirac superconductors: Second-order and boundary-obstructed topology, Phys. Rev. Research **2**, 043300 (2020).

[45] K. Asagaand and T. Fukui, Boundary-obstructed topological phases of a massive Dirac fermion in a magnetic field, Phys. Rev. B **102**, 155102 (2020).

[46] X. Wu, W. A. Benalcazar, Y. Li, R. Thomale, C.-X. Liu, and J. Hu, Boundary-Obstructed Topological High-t_c Superconductivity in Iron Pnictides, Phys. Rev. X **10**, 041014 (2020).

[47] L. Fidkowskiand and A. Kitaev, Effects of interactions on the topological classification of free fermion systems, Phys. Rev. B **81**, 134509 (2010).

[48] C. W. Peterson, W. A. Benalcazar, T. L. Hughes, and G. Bahl, A quantized microwave quadrupole insulator with topologically protected corner states, Nature (London) **555**, 346 (2018).

[49] A. J. Kollár, M. Fitzpatrick, and A. A. Houck, Hyperbolic lattices in circuit quantum electrodynamics, Nature (London) **571**, 45 (2019).

[50] S. Imhof, C. Berger, F. Bayer, J. Brehm, L. W. Molenkamp, T. Kiessling, F. Schindler, C. H. Lee, M. Greiter, T. Neupert, and R. Thomale, Topolectrical-circuit realization of topological corner modes, Nat. Phys. **14**, 925 (2018).

[51] Y. Deng, W. A. Benalcazar, Z.-G. Chen, M. Oudich, G. Ma, and Y. Jing, Observation of degenerate zero-energy topological states at disclinations in an acoustic lattice, arXiv:2112.05182.

[52] M. Aidelsburger, M. Atala, M. Lohse, J. T. Barreiro, B. Paredes, and I. Bloch, Realization of the Hofstadter Hamiltonian with Ultracold Atoms in Optical Lattices, Phys. Rev. Lett. **111**, 185301 (2013).

[53] H. Miyake, G. A. Siviloglou, C. J. Kennedy, W. C. Burton, and W. Ketterle, Realizing the Harper Hamiltonian with Laser-Assisted Tunneling in Optical Lattices, Phys. Rev. Lett. **111**, 185302 (2013).

[54] G. Jotzu, M. Messer, R. Desbuquois, M. Lebrat, T. Uehlinger, D. Greif, and T. Esslinger, Experimental realization of the topological haldane model with ultracold fermions, Nature (London) **515**, 237 (2014).

[55] M. Martinez, O. Giraud, D. Ullmo, J. Billy, D. Guéry-Odelin, B. Georgeot, and G. Lemarié, Chaos-Assisted Long-Range Tunneling for Quantum Simulation, Phys. Rev. Lett. **126**, 174102 (2021).

[56] I. Mondragon-Shem, T. L. Hughes, J. Song, and E. Prodan, Topological Criticality in the Chiral-Symmetric AIII Class at Strong Disorder, Phys. Rev. Lett. **113**, 046802 (2014).

[57] L. Lin, Y. Ke, and C. Lee, Real-space representation of the winding number for a one-dimensional chiral-symmetric topological insulator, Phys. Rev. B **103**, 224208 (2021).
[58] S. Velury, B. Bradlyn, and T. L. Hughes, Topological crystalline phases in a disordered inversion-symmetric chain, Phys. Rev. B **103**, 024205 (2021).
[59] See Supplemental Material at http://link.aps.org/supplemental/10.1103/PhysRevLett.128.127601 for details on the topological indices, the localization properties of the corner states, and the nature of transitions in these topological phases.
[60] R. Resta, Quantum-Mechanical Position Operator in Extended Systems, Phys. Rev. Lett. **80**, 1800 (1998).
[61] W. A. Wheeler, L. K. Wagner, and T. L. Hughes, Many-body electric multipole operators in extended systems, Phys. Rev. B **100**, 245135 (2019).
[62] B. Kang, K. Shiozaki, and G. Y. Cho, Many-body order parameters for multipoles in solids, Phys. Rev. B **100**, 245134 (2019).
[63] S. Ono, L. Trifunovic, and H. Watanabe, Difficulties in operator-based formulation of the bulk quadrupole moment, Phys. Rev. B **100**, 245133 (2019).
[64] R. Exeland and T. A. Loring, Invariants of almost commuting unitaries, J. Funct. Anal. **95**, 364 (1991).
[65] M. B. Hastingsand and T. A. Loring, Almost commuting matrices, localized Wannier functions, and the quantum Hall effect, J. Math. Phys. (N.Y.) **51**, 015214 (2010).
[66] B. Bradlyn, L. Elcoro, J. Cano, M. G. Vergniory, Z. Wang, C. Felser, M. I. Aroyo, and B. A. Bernevig, Topological quantum chemistry, Nature (London) **547**, 298 (2017).
[67] J. Cano, B. Bradlyn, Z. Wang, L. Elcoro, M. G. Vergniory, C. Felser, M. I. Aroyo, and B. A. Bernevig, Building blocks of topological quantum chemistry: Elementary band representations, Phys. Rev. B **97**, 035139 (2018).
[68] A. Agarwala, V. Juričić, and B. Roy, Higher-order topological insulators in amorphous solids, Phys. Rev. Research **2**, 012067(R) (2020).
[69] C.-A. Li, B. Fu, Z.-A. Hu, J. Li, and S.-Q. Shen, Topological Phase Transitions in Disordered Electric Quadrupole Insulators, Phys. Rev. Lett. **125**, 166801 (2020).
[70] Y.-B. Yang, K. Li, L.-M. Duan, and Y. Xu, Higher-order topological Anderson insulators, Phys. Rev. B **103**, 085408 (2021).
[71] F. Schindler, Z. Wang, M. G. Vergniory, A. M. Cook, A. Murani, S. Sengupta, A. Y. Kasumov, R. Deblock, S. Jeon, I. Drozdov *et al.*, Higher-order topology in bismuth, Nat. Phys. **14**, 918 (2018).
[72] R. Noguchi *et al.*, Evidence for a higher-order topological insulator in a three-dimensional material built from van der Waals stacking of bismuth-halide chains, Nat. Mater. **20**, 473 (2021).
[73] J. Noh, W. A. Benalcazar, S. Huang, M. J. Collins, K. P. Chen, T. L. Hughes, and M. C. Rechtsman, Topological protection of photonic mid-gap defect modes, Nat. Photonics **12**, 408 (2018).
[74] M. Serra-Garcia, R. Süsstrunk, and S. D. Huber, Observation of quadrupole transitions and edge mode topology in an LC circuit network, Phys. Rev. B **99**, 020304(R) (2019).
[75] H. Xue, Y. Yang, G. Liu, F. Gao, Y. Chong, and B. Zhang, Realization of an Acoustic Third-Order Topological Insulator, Phys. Rev. Lett. **122**, 244301 (2019).
[76] S. Mittal, V. V. Orre, G. Zhu, M. A. Gorlach, A. Poddubny, and M. Hafezi, Photonic quadrupole topological phases, Nat. Photonics **13**, 692 (2019).
[77] L. He, Z. Addison, E. J. Mele, and B. Zhen, Quadrupole topological photonic crystals, Nat. Commun. **11**, 3119 (2020).
[78] J. Bao, D. Zou, W. Zhang, W. He, H. Sun, and X. Zhang, Topoelectrical circuit octupole insulator with topologically protected corner states, Phys. Rev. B **100**, 201406(R) (2019).
[79] H. Xue, Y. Ge, H.-X. Sun, Q. Wang, D. Jia, Y.-J. Guan, S.-Q. Yuan, Y. Chong, and B. Zhang, Quantized octupole acoustic topological insulator, Nat. Commun. **11**, 2442 (2020).
[80] X. Ni, M. Li, M. Weiner, A. Alù, and A. B. Khanikaev, Demonstration of a quantized acoustic octupole topological insulator, Nat. Commun. **11**, 2108 (2020).
[81] L. He, Z. Addison, E. J. Mele, and B. Zhen, Quadrupole topological photonic crystals, Nat. Commun. **11**, 3119 (2020).
[82] Y. Ota, F. Liu, R. Katsumi, K. Watanabe, K. Wakabayashi, Y. Arakawa, and S. Iwamoto, Photonic crystal nanocavity based on a topological corner state, Optica **6**, 786 (2019).
[83] M. Proctor, P. A. Huidobro, B. Bradlyn, M. B. de Paz, M. G. Vergniory, D. Bercioux, and A. Garca-Etxarri, Robustness of topological corner modes in photonic crystals, Phys. Rev. Research **2**, 042038(R) (2020).
[84] W. Zhang, X. Xie, H. Hao, J. Dang, S. Xiao, S. Shi, H. Ni, Z. Niu, C. Wang, K. Jin, X. Zhang, and X. Xu, Low-threshold topological nanolasers based on the second-order corner state, Light Sci. Appl. **9**, 109 (2020).
[85] H.-R. Kim, M.-S. Hwang, D. Smirnova, K.-Y. Jeong, Y. Kivshar, and H.-G. Park, Multipolar lasing modes from topological corner states, Nat. Commun. **11**, 5758 (2020).